Thickness-dependent magnetic excitations in Permalloy films with nonuniform magnetization

J. Ben Youssef
LMB, CNRS-FRE 2697, UBO, 29285 Brest, France

N. Vukadinovic*
Dassault Aviation, 92552 St-Cloud, France

D. Billet and M. Labrune
LPMTM, CNRS-UPR 9001, Institut Galilée, Université Paris-13, 93430 Villetaneuse, France
(Received 25 November 2003; revised manuscript received 6 February 2004; published 4 May 2004)

The static and dynamic properties of Permalloy films with thicknesses varying from 200 nm to 920 nm have been investigated in detail. For these films possessing a perpendicular anisotropy, the critical thickness for stripe domain nucleation has been determined using magnetic force microscopy imaging and in-plane hysteresis loop measurements. The zero-field dynamic permeability spectra measured over the frequency range 0.1–6 GHz reveal one resonance line below the critical thickness, whereas multiple resonance peaks whose number increases with increasing film thickness are observed above the critical thickness. The two-dimensional dynamic micromagnetic simulations reproduce successfully the thickness evolution of the experimental permeability spectra and give access to the thickness-dependent spatial localization of the main modes. However, the experimental resonance linewidths exceed the computed ones for the thickest films. Extended dynamic micromagnetic simulations including the screening of the pumping field due to eddy currents account only partially for resonance line broadening. The existence of additional relaxation mechanisms due to magnetic inhomogeneities (micromagnetic and structural) is discussed on the basis of parallel ferromagnetic resonance measurements versus frequency.

DOI: 10.1103/PhysRevB.69.174402 PACS number(s): 75.40.Gb, 76.50.+g, 75.60.Ch, 75.70.−i

I. INTRODUCTION

During the past 40 years, extensive studies were devoted to the static and dynamic properties of low-anisotropy ferromagnetic films both from fundamental point of view and for numerous potential applications in magnetic storage media and microwave devices. Following the Hubert's classification,[1] these films can be distinguished by the type of anisotropy (in-plane or out-of-plane) and the film thickness range. Both the static magnetization configuration and the associated dynamic response are controlled by these key parameters. Permalloy films (Ni_xFe_{100-x}, with typically $78 \leqslant x \leqslant 82$) can be viewed as a prototype of such soft magnetic materials and represent an ideal system for basic investigations. The most commonly studied Permalloy films are characterized by near-zero magnetostriction ($x \simeq 81$),[2] vanishing magnetocrystalline anisotropy, and a weak in-plane uniaxial anisotropy induced by deposing the film in a polarizing magnetic field. The domain pattern is defined by large in-plane magnetization domains separated by various types of domain walls (Néel, cross-tie, asymmetric Néel, and Bloch walls) strongly depending on film thickness.[1] Another class of Permalloy films less investigated corresponds to the ones exhibiting a perpendicular anisotropy. This phenomenon is often observed in Ni-rich ($x > 81$) permalloy films and seems to originate from the magnetoelastic coupling in films with a negative magnetostriction constant and a planar tensile stress.[1] For Permalloy films with a perpendicular anisotropy, one of remarkable properties is the existence of a stripe domain pattern above a critical thickness as first observed in the early sixties.[3,4] From these pioneer works, such a stripe domain pattern (weak stripe type) was also successively evidenced in CoNbZr,[5] Co,[6] FeTaN,[7] CoFeZr,[8] and FePd[9] thin films, all exhibiting a perpendicular anisotropy. In the past few years, the dynamic response of thin films with a weak stripe domain structure was experimentally investigated using either zero-field microwave permeability [CoNbZr (Ref. 5) and CoFeZr (Ref. 8) thin films] or ferromagnetic resonance (FMR) measurements [Co (Refs. 10,11) and FePd (Ref. 12) thin films]. As a result, the magnetic excitation spectra exhibit multiple resonance peaks and depend on the pumping field orientation with respect to the stripe direction. On the other hand, it was demonstrated[13,14] that the two-dimensional (2D) dynamic micromagnetic simulations allow to reproduce such complex dynamic spectra and to interpret the resonance lines in terms of spatially localized modes within the stripe domain structure.

However, the dynamic response of Permalloy films developing a weak stripe domain structure has not been reported, to our knowledge, except some summary of experimental results.[15] The main purpose of this paper is to investigate both experimentally and theoretically the zero-field dynamic permeability spectra of Permalloy films possessing a perpendicular anisotropy as a function of film thickness.

This paper is organized as follows. In Sec. II, the sample preparation is described. Section III is devoted to the static magnetic properties and their thickness dependence. In particular, the critical thickness for stripe domain nucleation is determined using experimental methods [magnetic force microscopy (MFM) observations, in-plane hysteresis loop measurements]. The experimental and computed (mainly by 2D micromagnetic simulations) zero-field dynamic permeability

spectra for the two thickness regimes (below and above the critical thickness) are then reported in Sec. IV. A special attention is paid to the effect of eddy currents on the permeability spectra.

II. SAMPLE PREPARATION

A series of Permalloy ($Ni_{82}Fe_{18}$) thin films were grown on Corning glass substrate by rf diode sputtering using a standard Z550 Leybold equipment. A dc magnetic field of 300 Oe was applied parallel to the film plane during deposition in order to induce a well-defined uniaxial anisotropy. The background pressure was better than 3×10^{-7} mbar. Electron probe microanalyses carried out at several points on the samples revealed a uniform chemical homogeneity within $\pm1\%$. The thickness of the films determined by profilometer measurements was within the range from 200 nm to 920 nm. A SiO_2 capping layer of 2 nm was deposited to prevent the films from oxidation. The crystallographic structure of as-deposited films was examined by x-ray diffractometry with Cu $K\alpha$ radiation. The x-ray diagrams exhibited the diffraction spots of the $Ni_{82}Fe_{18}$ (111) and (200) fcc crystalline structure.

III. STATIC MAGNETIC PROPERTIES

A. In-plane hysteresis loops and MFM images versus film thickness

The saturation magnetization M_S and the in-plane hysteresis loops were measured using a vibrating sample magnetometer. The saturation induction was found equal to $4\pi M_S = 10\,390$ G. Figure 1 displays the in-plane hysteresis loops recorded on Permalloy films with different thicknesses. For the thinnest film ($t=204$ nm), a square loop is observed along the easy axis (EA) whereas a slightly tilted loop with a low value of the remanence appears along the in-plane hard axis (HA). These hysteresis loops are similar to those of classical in-plane uniaxial anisotropy films. The in-plane uniaxial anisotropy field H_{Kp} was determined from the in-plane saturation field along the HA, $H_{Kp}=4.8$ Oe which corresponds to an in-plane uniaxial anisotropy constant $K_p \equiv M_S H_{Kp}/2 \simeq 2\times10^3$ erg/cm^3. For the film thickness $t=327$ nm, the EA and HA hysteresis loops still differ but a curvature on the EA hysteresis loop near zero field accompanied with a small decrease of the remanence is observed. For larger film thicknesses $t=384$ nm and $t=596$ nm, two main features clearly appear.

(i) The in-plane hysteresis loops are characterized by a linear decrease of magnetization from its saturation value and a moderate remanence. This shape of the loops is typical of thin films with perpendicular anisotropy exhibiting a weak stripe domain structure.[4]

(ii) The EA and HA hysteresis loops are superimposed. More generally, the hysteresis loops are unchanged whatever the orientation of the applied in-plane magnetic field. This reflects the so-called rotatable anisotropy effect.[4]

From the four above-mentioned Permalloy films, the experimental critical thickness for rotatable anisotropy is estimated to be $t_{c,ra}=355\pm30$ nm. In addition, the in-plane hysteresis loops reveal that increasing film thickness leads to an increase of the coercive field and the in-plane saturation field whereas the value of the in-plane remanence is reduced.

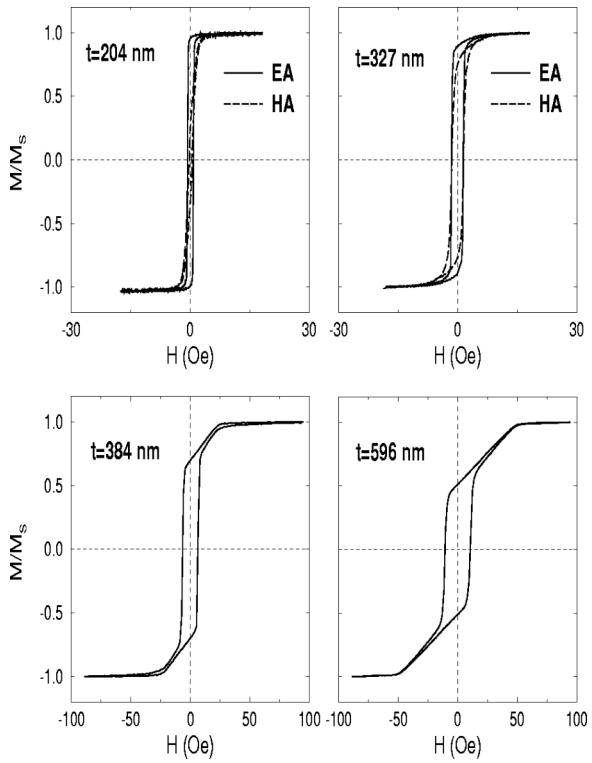

FIG. 1. Experimental in-plane hysteresis loops for different Permalloy film thicknesses.

The zero-field magnetic domain structure at the surface of the Permalloy films was then imaged by MFM—dimension 3100 apparatus. The interlace mode was used for the magnetic measurements using the phase detection system. The tips are magnetized along their axis (perpendicular to the film plane). Therefore, following the point-probe model under the dipolar approach,[16] the signal observed by MFM is expected to be proportional to the second derivative versus y (normal to the film plane) of the stray field component H_y. No magnetic contrast was detected for film thicknesses lower than $t=250$ nm. Within this thickness range, the static magnetization configuration observed by longitudinal Kerr microscopy consists of large domains with antiparallel magnetization (zero-field domain width $\simeq1$ mm for a sample with lateral dimensions 9 mm$\times$9 mm previously saturated along the EA) oriented along the in-plane easy axis. For film thickness exceeding $t=310$ nm, the MFM images reveal a parallel stripe domain structure (Fig. 2). This domain structure of weak stripe type is induced by first saturating the film in an in-plane dc magnetic field applied along the EA and then reducing the field to zero. The classical increase of the zero-field stripe period with increasing film thickness is found. From these observations, the critical thickness for magnetization reorientation corresponds to $t_{c,mr}=280\pm30$ nm. Knowing the critical thickness, it is possible to estimate the value of the perpendicular uniaxial anisotropy constant K_U using the phase diagram in the plane $(Q, t/\Lambda)$,[13] where Q is

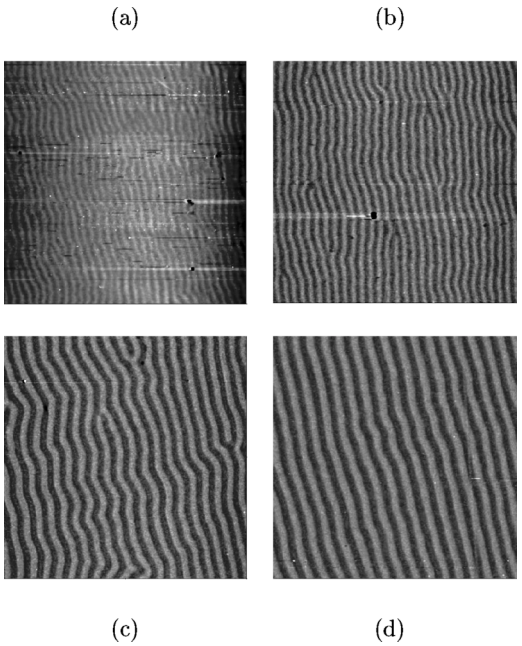

FIG. 2. Zero-field MFM images of the weak stripe domain structure as a function of film thickness: (a) $t=327$ nm, (b) $t=396$ nm, (c) $t=596$ nm, and (d) $t=917$ nm. The image sizes are 20 μm$\times$20 μm.

the quality factor defined as $Q=K_U/2\pi M_S^2$ and Λ the exchange length given by the expression $\Lambda=(A/2\pi M_S^2)^{1/2}$ with A the exchange constant. Assuming that K_U is independent of film thickness for this thickness range (hypothesis supported by the fact that no variation of magnetostriction coefficient is expected[17] and no thickness dependence of tensile stress was detected by x-ray diffraction measurements), this leads to $K_U=5\pm1.3\times10^4$ erg/cm^3 corresponding to the mean value of the quality factor $Q=0.012$. It should be mentioned that for this low-Q value, the relation $t_{c,mr}=2\pi\sqrt{A/K_u}$[1] provides an excellent approximation for determining K_U. Lastly, it should be also underlined that $t_{c,mr}$ was found lower than $t_{c,ra}$ in agreement with data previously reported.[4]

B. Equilibrium magnetization configuration above the critical thickness

Figure 3 exhibits the zero-field cross-sectional equilibrium magnetization configuration within one period of the weak stripe structure computed by 2D static micromagnetic simulations[18] for the film thicknesses $t=327$ nm and $t=917$ nm. As reported in Ref. 18 and verified in our system, for this class of magnetic films with a low quality factor the discretization rules for micromagnetic simulations can be relaxed and a 80×41 grid ensures the convergence of both static and dynamic micromagnetic computations. The value of the exchange constant $A=1\times10^{-6}$ erg/cm was adopted.[19] For the thinnest film near the critical line [Fig. 3(a)], the static magnetization configuration can be viewed as an accumulation along the x axis of vortexlike domain walls with alternate flux circulations. Increasing film thickness leads to the development of up and down magnetized domains separated by a Bloch-type domain wall at the film center surrounded by closure domains at film surfaces as observed in Fig. 3(b). According to the lift scan height of the magnetic tip over the film plane the bright and dark areas can be regarded as corresponding to the position of the inner up and down domains.[6,20]

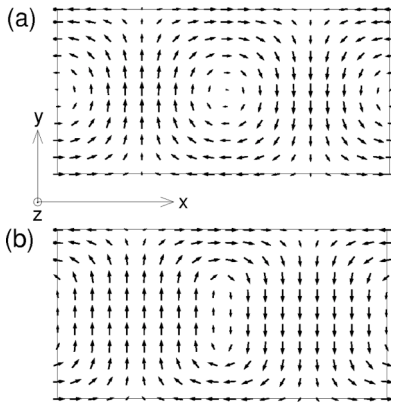

FIG. 3. Cross-sectional equilibrium magnetization distribution over one period of the weak stripe pattern computed by 2D static micromagnetic simulations. The arrows represent the component of **M** in the plane (Ox,Oy) of the figure perpendicular to the direction (Oz) of the stripe domains: (a) $t=327$ nm, and (b) $t=917$ nm.

Figure 4 shows the comparison between the experimental and computed variations of the in-plane longitudinal remanent magnetization M_r/M_S [Fig. 4(a)], in-plane saturation field H_{sat} [Fig. 4(b)], and the zero-field stripe period P_0 [Fig. 4(c)] as a function of film thickness. The good agreement obtained between experiment and theory indicates the consistency of the static magnetic parameters.

IV. ZERO-FIELD MICROWAVE PERMEABILITY SPECTRA

The effect of film thickness on the zero-field microwave permeability spectra was analyzed in detail both experimentally and theoretically. From the experimental point of view, the complex scalar dynamic permeability $\mu\equiv\mu'-i\mu''$ (μ' and μ'' are the real and imaginary parts of μ, respectively) was measured over the frequency range 0.1–6 GHz using a single coil permeameter.[21] This broadband technique is based on the measurements of the input impedance of the coil with and without the sample. The mean flux variation introduced by the ferromagnetic film induces a coil impedance variation from which the dynamic permeability is determined. This technique requires a sample with lateral dimensions 9 mm$\times$9 mm. The experimental spectra were then compared with those computed by means of either an analytical model or 2D dynamic micromagnetic simulations.[13,14]

A. Below the critical thickness

Figure 5 shows the imaginary part of zero-field scalar dynamic permeability spectra for a Permalloy film whose thickness ($t=204$ nm) is lower than the critical thickness ($t_{c,mr}\simeq280$ nm). For this in-plane magnetized film, the experimental dynamic permeability spectrum (dashed line)

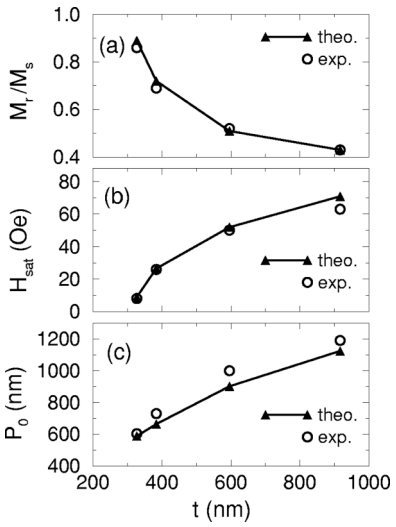

FIG. 4. Thickness evolution of static magnetic parameters deduced from experiment (open circles) and computed by 2D micromagnetic simulations (solid lines with symbols): (a) reduced in-plane longitudinal remanent magnetization M_R/M_S, (b) in-plane saturation field H_{sat}, and (c) zero-field stripe period P_0.

measured along the in-plane HA (x axis) exhibits, as expected, one resonance corresponding to the so-called in-plane uniform gyromagnetic mode. This resonance line is characterized by the following parameters: the resonance frequency $f_r \simeq 600$ MHz, the resonance linewidth (full width at half maximum) $\Delta f_r \simeq 490$ MHz, and the maximum of μ'', $\mu''_{max} \simeq 2400$.

It is well known[22] that the HA intrinsic permeability spectrum of an in-plane magnetized thin film can be computed by solving the Landau-Lifshitz-Gilbert (LLG) equation for magnetization motion under the following approximations.

(i) The film thickness is very small in comparison with the film lateral dimensions.

(ii) The film is assumed homogeneously in-plane magnetized. Although the zero-field magnetization configuration consists of a multidomain state with large domains oriented along the easy axis, this approximation is relevant since the film thickness remains very small with respect to the domain width.

(iii) The effective field including the contributions of anisotropy and demagnetizing fields is also considered as uniform. The demagnetizing field is computed by analogy to the one of an ellipsoid of revolution with the demagnetizing factor equaling 1 along the film normal and 0 for the transverse directions.

(iv) The amplitudes of the pumping field $\delta\mathbf{h}$ and the dynamic magnetization $\delta\mathbf{m}$ are small in comparison with the ones of the static effective field and the static magnetization, respectively (linear regime).

(v) The damping parameter is small with respect to unity. By taking into account both the in-plane H_{Kp} and perpendicular H_{Ku} anisotropy fields, this leads to the classical expression for the HA intrinsic permeability to first order in α:

$$\mu_{HA}^{int} = 1 + \gamma^2 4\pi M_S \frac{[H_{Kp} - H_{Ku} + 4\pi M_S + i\alpha\omega/\gamma]}{\omega_r^2 - \omega^2 + i\omega\Delta\omega_r}, \quad (1)$$

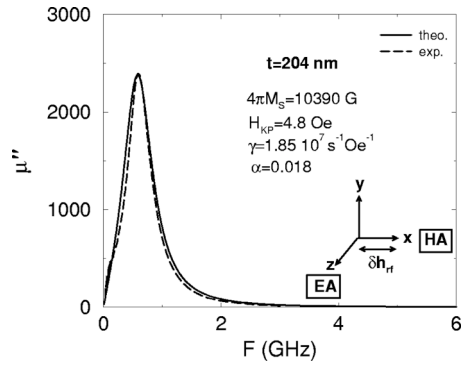

FIG. 5. Imaginary part of zero-field permeability spectra for an in-plane magnetized Permalloy film ($t < t_{c,mr}$). The pumping field $\delta\mathbf{h}$ is applied along the in-plane hard axis (HA). Experiment (dashed line) and best fit according Eq. (1) (solid line) corresponding to the Gilbert damping parameter $\alpha = 0.018$.

with

$$(\omega_r/\gamma)^2 = H_{Kp}[H_{Kp} - H_{Ku} + 4\pi M_S], \quad (2)$$

and

$$\Delta\omega_r = \alpha\gamma[2H_{Kp} - H_{Ku} + 4\pi M_S]. \quad (3)$$

The expressions (1), (2), and (3) are valid only for $H_{Ku} < H_{Kp} + 4\pi M_S$. This inequality ensures that the film remains in-plane magnetized. For Permalloy films satisfying $H_{Ku} \ll 4\pi M_S$, the angular resonance frequency [Eq. (2)] and the resonance linewidth [Eq. (3)] are very weakly dependent on H_{Ku}. The effective permeability including the effect of eddy currents can be written as[23]

$$\mu_{HA} = \mu_{HA}^{int} \frac{\tanh[(1+i)t/(2\delta)]}{(1+i)t/(2\delta)}, \quad (4)$$

with δ the skin depth defined as $\sqrt{2\rho/(\omega\mu_0\mu_{HA}^{int})}$, where ρ is the electrical resistivity and μ_0 the permeability of free space. Equation (4) was used in order to fit the experimental HA permeability spectrum. The computation was made using the static magnetic parameters reported in Sec. III and the value of the gyromagnetic ratio deduced from FMR measurements, $\gamma = 1.85 \times 10^7$ s^{-1} Oe^{-1}. The Gilbert damping term was considered as a free parameter. The best computed permeability spectrum is represented in Fig. 5 (solid line) and corresponds to $\alpha = 0.018$. This value is consistent with the one previously reported[15] and obtained by the same technique on a Permalloy film of equivalent thickness. For the film thickness under consideration, the eddy currents have a moderate influence on the intrinsic permeability spectrum (mainly a reduction of μ''_{max} by 10%) using the value of the Permalloy resistivity $\rho = 25$ $\mu\Omega$ cm.[19] It should be mentioned that the dynamic permeability spectrum recorded for the pumping field applied along the EA (z axis) reveals a small amplitude signal with a resonant shape. The resonance frequency coincides with the one obtained for HA permeability spectrum and $\mu''_{max,EA} \simeq 100$. The existence of a very weak dispersion in the in-plane anisotropy direction can explain the occurrence of the EA permeability response.

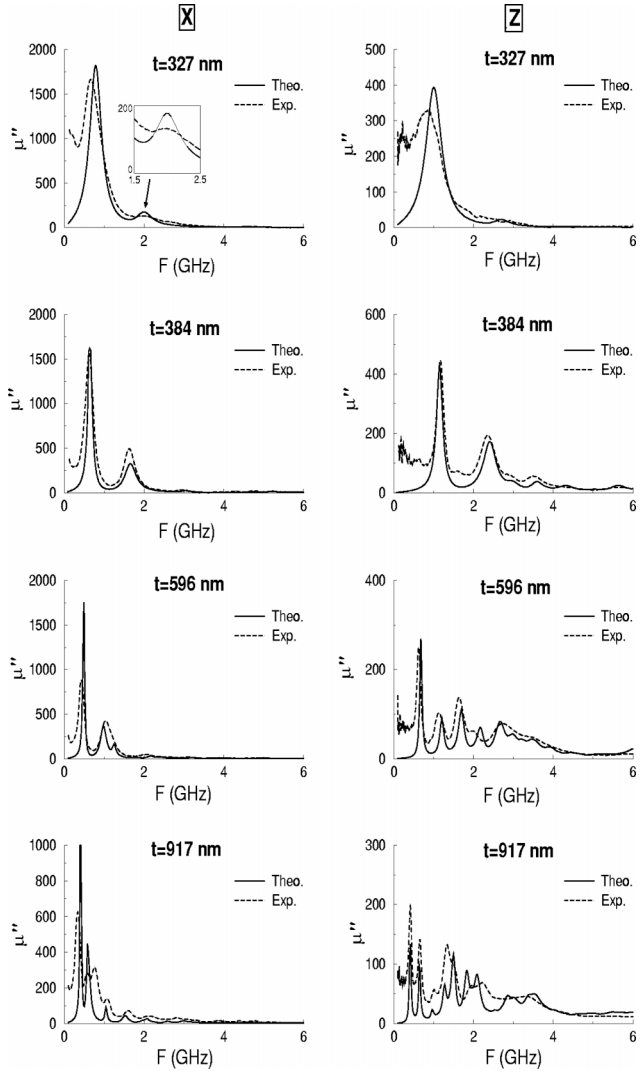

FIG. 6. Comparison between computed (solid lines) and experimental (dashed lines) zero-field scalar dynamic susceptibility spectra (imaginary part) for Permalloy thin films with different thicknesses above the transition line. The pumping field is applied in the film plane either perpendicular (X configuration, left column) or parallel (Z configuration, right column) to the stripe direction.

B. Above the critical thickness

1. Experiment versus 2D dynamic micromagnetic simulations

Zero-field microwave permeability measurements were then performed on the thin films possessing a weak stripe domain structure in the frequency range 0.1–6 GHz. The stripe domains were oriented by means of an in-plane polarizing magnetic field whose amplitude exceeds the in-plane saturated field and is then reduced to zero. Two orientations of the pumping field were considered $\delta\mathbf{h}$ perpendicular to the stripe direction, and $\delta\mathbf{h}$ parallel to the stripe direction. By taking the z axis as the stripe direction, the configurations are denoted, respectively, by X configuration and Z configuration. The experimental scalar dynamic permeability spectra (imaginary part) for each pumping configuration and for four film thicknesses are reported in Fig. 6 (dashed lines). In contrast to the dynamic permability spectrum of the film with thickness below the critical line (Fig. 5), these spectra show multiple resonance peaks and a significant longitudinal response (Z configuration). More precisely, these spectra reveal clearly some striking features which can be described as follows.

Increasing film thickness leads to the following.

(i) An increase of the number of the magnetic resonances. Up to seven peaks are detected for the thickest film.

(ii) A shift of the main resonances towards the low frequencies for the X configuration. This behavior appears also for the Z configuration but the variation is not monotonic.

(iii) A decrease of the permeability level (imaginary part) for both the X and Z configurations.

(iv) A drastic reduction of the resonance linewidths.

It should be mentioned that the permeability variations below 200 MHz are affected by experimental noise and are not representative.

The permeability spectra were compared with those computed using a 2D dynamic micromagnetic model first by neglecting the effect of eddy currents. This model, described elsewhere,[13,14] is based on the solution of the Landau-Lifshitz-Gilbert equation for magnetization motion linearized around the equilibrium configuration and gives access to the full dynamic susceptibility tensor $\overline{\overline{\chi}}$ (permeability tensor $\overline{\overline{\mu}} = \overline{\overline{I}} + 4\pi\overline{\overline{\chi}}$, where $\overline{\overline{I}}$ is the unit tensor) for nonuniform and periodic equilibrium magnetization configurations. A very good agreement between theory and experiment was previously reported for an amorphous CoFeZr thin film with magnetic parameters $Q = 0.05$ and $t/\Lambda = 68$.[13] For the Permalloy films under consideration, these parameters correspond to $Q \simeq 0.012$ and t/Λ varies between 68 and 190. The computations were performed using the magnetic parameters determined previously (see Secs. III and IV A).

The computed permeability spectra are shown in Fig. 6 (solid lines). As a result, the 2D dynamic micromagnetic model reproduces very well the thickness evolution of the permeability spectra described above by the items (i–iv). For the thicknesses $t = 327$ nm and $t = 384$ nm, a very good agreement is found in terms of mode positions, permeability levels, and resonance linewidths. For the two largest thicknesses ($t = 596$ nm and $t = 917$ nm), the computations account for accurately the complicated permeability spectra with multiple resonance peaks. Nevertheless, it should be emphasized that the resonance linewidths appear smaller than the experimental ones. Consequently, this leads to the prediction of some resonance peaks not fully resolved by the permeability measurements. In addition, the permeability levels of the main resonance for the X configuration are overestimated with respect to experiment. The broadening of the experimental resonance lines can be originated mainly from two causes: (i) the effect of eddy currents, and (ii) a thickness dependence of the magnetization relaxation through intrinsic or extrinsic processes. These different causes will be discussed in Sec. IV B 3.

2. Thickness dependence of the main resonance modes

It was shown previously[13] that the resonance peaks appearing in low-Q magnetic films can be correlated with the

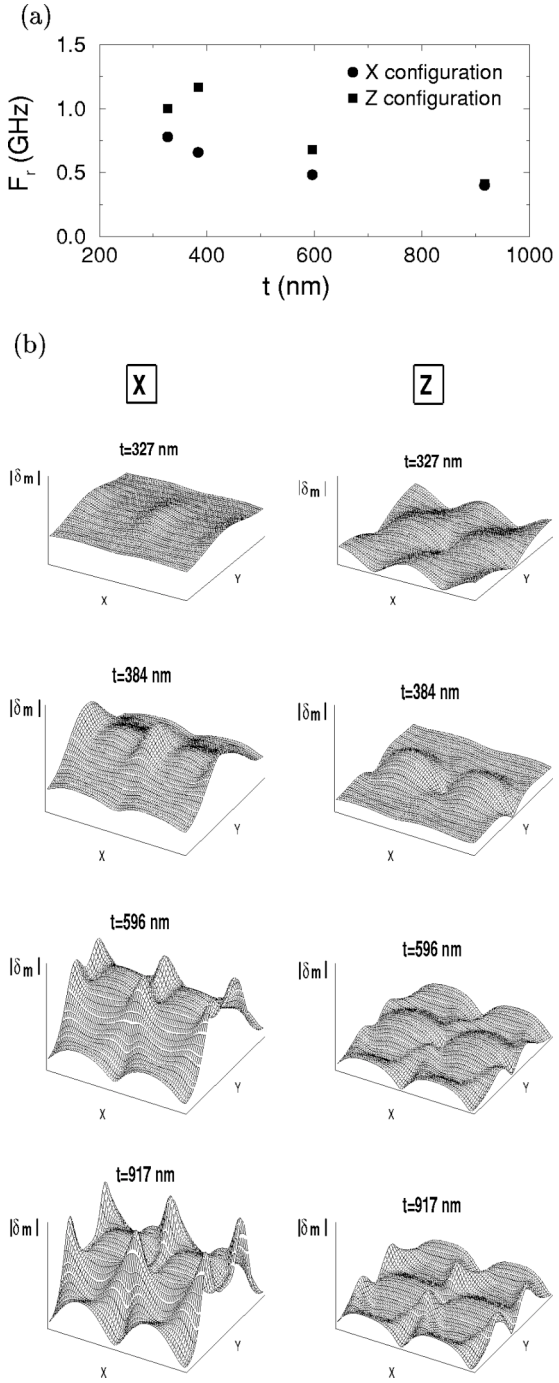

FIG. 7. Computed thickness evolution of the low-frequency magnetic excitation observed in Fig. 6 for the *X* and *Z* configurations: (a) resonance frequency, and (b) spatial distribution of $|\delta\mathbf{m}|$ within one period at each resonance frequency. For each column, the scale for $|\delta\mathbf{m}|$ is the same for all the maps.

excitation of different spin regions (parts of domains, closure domains, and domains walls) of the stripe structure. One way to identify these spin regions is to visualize the modulus of the dynamic magnetization $\delta\mathbf{m}$ within one period of stripe domains at each resonance frequency. In this work, we are focused on the low-frequency and high-intensity resonance associated with each exciting configuration. Figure 7(a) represents the evolution of the respective resonance frequency as a function of film thickness. For each resonance frequency and each exciting configuration, the map of $|\delta\mathbf{m}(x,y)|$ is plotted in Fig. 7(b). For the *X* configuration, $|\delta\mathbf{m}|$ appears quite homogeneous for the thinnest film. A smooth maximum is observed within the domain wall at the film center. For this film thickness near the critical line, the spatial distribution of $|\delta\mathbf{m}|$ does not depart significantly from the constant one occurring for films with in-plane magnetization below the transition line. As the film thickness increases, the dynamic magnetization becomes more and more heterogeneous. The maximum of $|\delta\mathbf{m}|$ within the domain wall is splitted into two maxima located symmetrically with respect to the film center. The distance between these maxima enhances with increasing film thickness. For the *Z* configuration, $|\delta\mathbf{m}|$ is found heterogeneous even for the thinnest film. In this case, the high values of $|\delta\mathbf{m}|$ correspond to the central parts of domains and to the closure areas. The more the increase in the film thickness, the more complicated the map of modes is. The central parts of domains remain a spin area with large values of $|\delta\mathbf{m}|$ whatever the film thickness, whereas the values of $|\delta\mathbf{m}|$ decrease within the closure areas and increase at the surfaces of domains with increasing film thickness. For the thickest films, the two maxima located symmetrically with respect to the film center emerge as observed for the *X* configuration.

3. Analysis of resonance linewidths

The existence of eddy currents in ferromagnetic films has been recognized for a long time as a possible source of line broadening for high-frequency magnetic excitations.[24,25] Due to the eddy currents, the pumping field becomes heterogeneous along the film thickness which induces a restoring torque arising from the exchange interaction (exchange-conductivity mechanism). Numerous papers were devoted to the analysis of the effect of eddy currents on FMR spectra for uniformly magnetized thin films.[26] It was shown that the exchange-conductivity mechanism produces a shift of the resonance field and an increase of the resonance linewidth for both parallel and perpendicular FMR configurations. Furthermore, the roles played by the boundary conditions (surface magnetic anisotropy) and the film thickness were analyzed in detail.[26–29] The second problem classically treated in the literature is the effect of eddy current losses on an isolated domain wall motion.[1,30,31] The existence of eddy currents leads to a decrease of the domain wall mobility with increasing film thickness and to a bulging of the domain wall during its motion. More generally, the problem of eddy currents for a nonuniform magnetization configuration is quite complex and requires the simultaneous solution of the LLG equation and the Maxwell equations.[32] Such a computation was reported recently[33] but it is outside the scope of this paper. In our case, this rigorous treatment would lead to a 2D eddy current magnetic field distribution due to the 2D static magnetization and effective field. In this paper, a simplified approach was adopted. In order to account for the screening of the pumping magnetic field by the eddy currents, a one-dimensional decrease of the pumping field between the surfaces and the center of the film was considered. For the case of a pumping field oriented along the *x* direction, and assum-

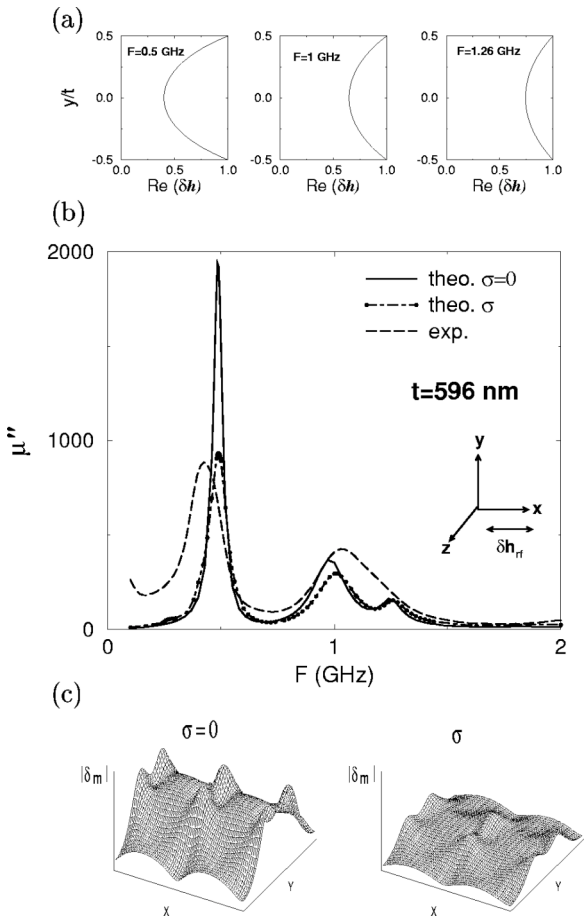

FIG. 8. (a) Pumping field profiles across the film thickness deduced from Eq. (5). These profiles are computed at the resonance frequencies associated with the first three modes of the theoretical spectrum corresponding to the film thickness $t=596$ nm and the X pumping field configuration (see Fig. 6 first column, third row). (b) Comparison between the theoretical dynamic permeability spectra (imaginary part) computed without ($\sigma=0$) and with (σ) eddy currents, and the experimental one. (c) Spatial distribution of $|\delta\mathbf{m}|$ within one period at the resonance frequency of the low-frequency peak without ($\sigma=0$) and with (σ) eddy currents. The mode representation is the same as in Fig. 6(b) and the scale is the same for the two maps.

ing an infinite film in the x and z directions, the solution of Maxwell equations using symmetrical boundary conditions at film surfaces yields the following profile for an unitary external pumping field:[34]

$$\delta h_x(y)=\frac{\cosh[(1+i)y/\delta]}{\cosh[(1+i)t/(2\delta)]}, \tag{5}$$

where the value of the permeability tensor element μ_{xx} computed from dynamic micromagnetic simulations and averaged over the periodic cell is incorporated in the expression of the skin depth δ. This pumping field profile was then included in the dynamic micromagnetic simulations. It should be noted that other nonuniform exciting field profiles representative of different magnetic couplings were recently investigated in the case of dynamic micromagnetic simulations on FePd thin films.[35] Figure 8 shows the results obtained for the film thickness $t=596$ nm and for the X configuration. Figure 8(a) reports the pumping field profile along the film thickness computed using Eq. (5) at the three resonance frequencies of the permeability spectrum. The maximum screening of the pumping field occurs at the first resonance frequency. The consequences on the permeability spectrum are displayed in Fig. 8(b). The effect of eddy currents results in a strong reduction of the first peak amplitude with correlatively an increase of the resonance linewidth by a factor of 2. However, a significative discrepancy subsists between the experimental and theoretical linewidths. The secondary peaks are weakly affected by the eddy currents. The effect of eddy currents cannot explain the experimental observation of a single broad secondary peak instead of the two peaks predicted by the dynamic micromagnetic simulations. Figure 8(c) compares the map of $|\delta\mathbf{m}|$ within the periodic cell for the low-frequency resonance without and with eddy currents. As expected, the presence of eddy currents induces a large decrease of $|\delta\mathbf{m}|$ mainly observed at the film center where the amplitude of the pumping field is minimum. The computations performed for the Z configuration indicate no significative change of the dynamic permeability spectrum associated with the eddy currents due to the lower permeability level. Despite the approximate treatment used, the dynamic micromagnetic simulations including the effect of eddy currents improve notably the comparison between theory and experiment but cannot fully explain the experimental resonance linewidths.

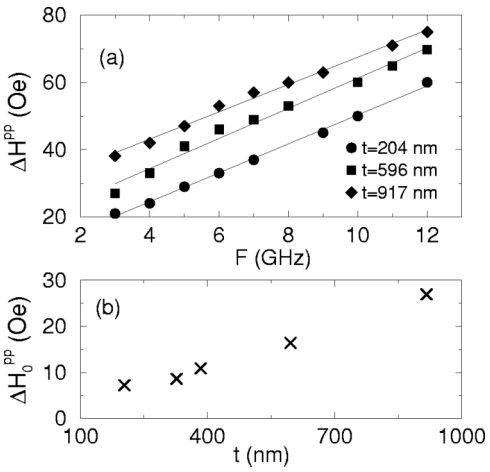

FIG. 9. (a) Evolution of the peak-to-peak linewidth ΔH^{pp} as a function of frequency for various film thicknesses. The symbols are FMR data and the solid lines represent the linear fits. (b) Thickness dependence of the zero-frequency peak-to-peak linewidth $\Delta H_0{}^{pp}$.

In order to gain a better understanding of the observed discrepancy between experimental and computed thickness dependences of resonance linewidths, FMR measurements were made for all the samples. The FMR investigations were performed in the saturated regime using a nonresonant wideband microstrip line in the frequency range 3–12 GHz with the polarizing magnetic field applied in the film plane (parallel FMR). Figure 9(a) shows the frequency evolution of the peak-to-peak parallel resonance linewidth ΔH^{pp}, defined as the field separation between the peaks of absorption deriva-

tive. For the sake of clarity, only three representative film thicknesses are reported. Several conclusions can be drawn.

(i) ΔH^{pp} increases linearly with frequency. Such a behavior is in agreement with previous results obtained for thinner Permalloy films.[36–38] In this thickness range, no significant variation of the slope is observed and the Gilbert damping parameter α deduced from the relationship[39] $\Delta H^{pp}=\Delta H_0^{pp}+2\alpha\omega/(\gamma\sqrt{3})$ is estimated to be $\alpha=1.1\pm0.1\times10^{-2}$. This value is similar to the one recently determined from angular measurements of FMR.[40]

(ii) The value of α is 40% lower than the one obtained by fitting the zero-field permeability spectrum of the in-plane magnetized thin film (see Fig. 5). The presence of multidomain state could explain the enhancement of the damping parameter as reported for insulator magnetic oxides.[41] More generally, it could be concluded that the damping parameter is intimately connected to the micromagnetic state of films. For the thickest films with a weak stripe domain structure, the highly heterogeneous static micromagnetic configurations could lead to a further enhancement of α. Introduction of such an increasing function $\alpha(t)$ into the dynamic micromagnetic simulations would improve the agreement between experimental and computed frequency linewidths for the thickest films.

(iii) The peak-to-peak zero-frequency linewidth ΔH_0^{pp} is an increasing function of film thickness. This term reflects the structural quality of samples. The origin of ΔH_0^{pp} was mainly attributed to anisotropy dispersion[39] and to the two-magnon scattering process which is operative for parallel FMR.[36,37]

In the last case, increasing film thickness leads to an increase of the number of states degenerated with the uniform precession mode and hence reinforced the two-magnon scattering contribution. Such an extrinsic contribution, not taken into account by the dynamic micromagnetic simulations, could also explain the discrepancy between the experimental and computed frequency linewidths for the thickest films.

From the above considerations, it is likely that the resonance line broadenings in the zero-field dynamic permeability spectra of the thickest Permalloy films arise partly from eddy currents and partly from relaxation processes related to magnetic inhomogeneities (micromagnetic and structural).

V. SUMMARY AND CONCLUSION

The static and dynamic properties of Permalloy films with thicknesses varying from 200 nm to 920 nm have been investigated in detail. For these films possessing a perpendicular anisotropy, the transition of reorientation (in-plane to out-of-plane magnetization) has been analyzed by means of in-plane hysteresis loops and MFM observations giving access to the critical thickness for the presence of stripe domains. The zero-field dynamic permeability spectra measured in the frequency range 0.1–6 GHz reveal one resonance line corresponding to the in-plane uniform gyromagnetic mode below the critical thickness and multiple resonance peaks associated with localized modes of stripe domains above the critical thickness. Increasing film thickness leads to an increase of resonance line number and to a reduction of resonance linewidths. The 2D dynamic micromagnetic simulations reproduce successfully these features and appear as a relevant approach for analyzing the high frequency response of Permalloy films in a wide thickness range. However, the experimental resonance linewidths exceed those computed for the thickest films. In this case, the introduction of the effect of eddy currents into the dynamic micromagnetic simulations leads to a significant reduction of the main peak amplitude in agreement with experiment but cannot account for the full experimental resonance linewidth. In order to understand the origin of this discrepancy, parallel FMR measurements versus frequency and film thickness were performed. As a result, the damping parameter obtained in saturated regime is smaller than the one determined from zero-field microwave permeability spectra. A correlation between the damping parameter and the micromagnetic state of films is suggested, which could result in an increase of the damping parameter with film thickness (increase of micromagnetic state inhomogeneity) and could partly explain the difference between the experimental and computed frequency linewidths in the zero-field permeability spectra for the thickest films. It would be interesting to test experimentally this assumption in the case of submicron magnetic objects where well-controlled micromagnetic states can be stabilized.[42] Finally, the existence of additional extrinsic relaxation mechanisms (two magnons scattering, weak anisotropy dispersion) is advanced on the basis of the increase of the zero-frequency linewidth with increasing film thickness. Such an extrinsic contribution not included in the dynamic micromagnetic simulations could provide an alternate explanation of the discrepancy between the experimental and computed frequency linewidths in the zero-field permeability spectra for the thickest films. The effects of anisotropy dispersion on the dynamic properties of magnetic films have been experimentally investigated recently.[43] The introduction of the fluctuations in the effective field (spatially varying anisotropy field)[44] into the micromagnetic simulations would provide a deeper insight on the complicated problem of damping mechanisms in real magnetic films.

ACKNOWLEDGMENTS

The authors thank D. Dekadjevi and J. Ostorero for stimulating discussions on x-ray-diffraction measurements and A. Thiaville for Kerr microscopy imaging.

*Corresponding author. Email address: nicolas.vukadinovic@dassault-aviation.fr

[1] A. Hubert and R. Schaefer, *Magnetic Domains* (Springer, Heidelberg, 1998).
[2] E. Klokholm and J.A. Aboaf, J. Appl. Phys. **52**, 2474 (1981).
[3] R.J. Spain, Appl. Phys. Lett. **3**, 208 (1963).
[4] N. Saito, H. Fujiwara, and Y. Sugita, J. Phys. Soc. Jpn. **19**, 1116 (1964).
[5] Y. Shimada, M. Shimoda, and O. Kitakami, Jpn. J. Appl. Phys., Part 1 **34**, 4786 (1995).

[6] M. Hehn, S. Padovani, K. Ounadjela, and J.P. Bucher, Phys. Rev. B **54**, 3428 (1996).
[7] B. Viala, M.K. Minor, and J.A. Barnard, J. Appl. Phys. **80**, 3941 (1996).
[8] O. Acher, C. Boscher, B. Brulé, G. Perrin, N. Vukadinovic, G. Suran, and H. Joisten, J. Appl. Phys. **81**, 4057 (1997).
[9] V. Gehanno, R. Hoffmann, Y. Samson, A. Marty, and S. Auffret, Eur. Phys. J. B **10**, 457 (1999).
[10] U. Ebels, P.E. Wigen, and K. Ounadjela, Europhys. Lett. **46**, 94 (1999).
[11] U. Ebels, L. Buda, K. Ounadjela, and P.E. Wigen, Phys. Rev. B **63**, 174437 (2001).
[12] N. Vukadinovic, H. Le Gall, J.B. Youssef, V. Gehanno, A. Marty, Y. Samson, and B. Gilles, Eur. Phys. J. B **13**, 445 (2000).
[13] N. Vukadinovic, O. Vacus, M. Labrune, O. Acher, and D. Pain, Phys. Rev. Lett. **85**, 2817 (2000).
[14] N. Vukadinovic, M. Labrune, J. Ben Youssef, A. Marty, J.C. Toussaint, and H.L. Gall, Phys. Rev. B **65**, 054403 (2002).
[15] E. Moraitakis, L. Kompotiatis, M. Pissas, and D. Niarchos, J. Magn. Magn. Mater. **222**, 168 (2000).
[16] U. Hartmann, Phys. Lett. A **137**, 475 (1989).
[17] Y.K. Kim and T.J. Silva, Appl. Phys. Lett. **68**, 2885 (1996).
[18] M. Labrune and J. Miltat, J. Appl. Phys. **75**, 2156 (1994).
[19] N. Smith, D. Markham, and D.L. Tourette, J. Appl. Phys. **65**, 4362 (1989).
[20] M. Labrune and L. Belliard, Phys. Status Solidi A **174**, 483 (1999).
[21] D. Pain, M. Ledieu, O. Acher, A.L. Adenot, and F. Duverger, J. Appl. Phys. **85**, 5151 (1999).
[22] C. Vittoria, *Microwave Properties of Magnetic Materials* (Springer, London, 1993).
[23] E. van de Riet and F. Roozeboom, J. Appl. Phys. **81**, 350 (1997).
[24] C. Kittel and C. Herring, Phys. Rev. **77**, 725 (1950).
[25] W.S. Ament and G.T. Rado, Phys. Rev. **97**, 1558 (1955).
[26] Z. Frait and D. Fraitova, in *Frontiers in Magnetism of Reduced Dimension Systems*, Vol. 49 of *NATO Advanced Study Institute, Series C: Mathematical and Physical Sciences*, edited by V. G. Bar'yakhtar, P. E. Wigen, and N. A. Leisnik (Kluwer, Dordrecht, 1998).
[27] C. Vittoria, R.C. Barker, and A. Yelon, J. Appl. Phys. **40**, 1561 (1969).
[28] C. Vittoria, G.C. Bayley, R.C. Barker, and A. Yelon, Phys. Rev. B **7**, 2112 (1973).
[29] G.C. Bayley and C. Vittoria, Phys. Lett. **37A**, 261 (1972).
[30] C.E. Patton, T.C. McGill, and C.H. Wilts, J. Appl. Phys. **37**, 3594 (1966).
[31] H.T. Wang and S.T. Chui, Phys. Rev. B **60**, 12 219 (1999).
[32] L. Kraus, J. Magn. Magn. Mater. **195**, 764 (1999).
[33] G.M. Sandler and H.N. Bertram, J. Appl. Phys. **81**, 4513 (1997).
[34] R. L. Stoll, *The Analysis of Eddy Currents* (Clarendon, Oxford, 1974).
[35] A. Marty, J. C. Toussaint, and N. Vukadinovic, Colloque Louis Néel (2002).
[36] A.J. Bertaud and H. Pascard, J. Appl. Phys. **36**, 970 (1965).
[37] C.E. Patton, J. Appl. Phys. **39**, 3060 (1968).
[38] C.E. Patton, Z. Frait, and C.H. Wilts, J. Appl. Phys. **46**, 5002 (1975).
[39] R.H. Nelson, J. Appl. Phys. **35**, 808 (1964).
[40] J. Dubowik and F. Stobiecki, J. Magn. Magn. Mater. **242-245**, 538 (2002).
[41] T. Taffary, D. Autissier, F. Boust, and H. Pascard, IEEE Trans. Magn. **34**, 1384 (1998).
[42] J. Kin Ha, R. Hertel, and J. Kirschner, Phys. Rev. B **67**, 224432 (2003).
[43] J. McCord and J. Paul, IEEE Trans. Magn. **39**, 2359 (2003).
[44] R.D. McMichael, D.J. Twisselmann, and A. Kunz, Phys. Rev. Lett. **90**, 227601 (2003).